Magazine of Concrete Research
Volume 65 Issue 3

Non-linear analysis of reinforced concrete walls under three-dimensional loading
Mullapudi and Ayoub

Magazine of Concrete Research, 2013, **65**(3), 172–184
http://dx.doi.org/10.1680/macr.12.00038
Paper 1200038
Received 14/02/2012; revised 04/05/2012; accepted 09/05/2012
Published online ahead of print 30/11/2012

ice Institution of Civil Engineers
publishing

Non-linear analysis of reinforced concrete walls under three-dimensional loading

Taraka Ravi Shankar Mullapudi
Senior Staff Engineer, MMI Engineering Inc., Houston, USA

Ashraf Ayoub
Professor of Civil Engineering, School of Engineering and Mathematical Sciences, City University London, London, UK

Analytical studies are conducted to develop an effective analytical model to simulate the non-linear response of reinforced concrete (RC) walls subjected to three-dimensional (3D) loads. The interaction between the concrete and steel is taken into account with consideration of the smeared behaviour of steel and tension stiffening of concrete. The proposed model is formulated to address the interaction between the axial force, shear, bending and torsion loads. The shear mechanism along the beam is modelled by adopting a Timoshenko beam approach for 3D frame elements with arbitrary cross-section geometry. The non-linear behaviour of the composite element is derived entirely from the constitutive laws of concrete and steel. The concrete constitutive model follows the softened membrane model that predicts the tensile cracking, compression crushing, strain softening, steel yielding and material damage under combined loadings. The validity of the model is established through a correlation study of experimentally tested RC shear walls subjected to monotonic loading conditions.

Notation

f'_c	uniaxial concrete compressive strength
f_{sx}, f_{sy}, f_{sz}	reinforcing bar stresses along the x, y and z directions
K_{c1}, K_{c2}, K_{c3}	biaxial strength magnification factors in 1–2–3 directions
$[R(\alpha_1)]$	rotating matrix
$\boldsymbol{S}(x) = \{N\ V\ W\ T\ M_y\ M_z\}^T$	section forces
$\{s\} = \{\varepsilon_0\ \chi_y\ \chi_z\ \chi_x\ \gamma_{xy0}\ \gamma_{xz0}\}^T$	section deformations
$[T]$	transformation matrix
$\{u_0\ v_0\ w_0\ \theta_x\ \theta_y\ \theta_z\}^T$	frame displacements in global system
x–y–z	global coordinates of reinforced concrete element
1–2–3	direction of applied principal tensile stress
$[\alpha_1]$	angle between (x–y–z) coordinate system and (1–2–3) coordinate system
α^*_{r1}	deviation angle between applied stress angle α_1 and rotating angle α_r
$\{\varepsilon\} = \{\varepsilon_x\ \gamma_{xy}\ \gamma_{xz}\}^T$	available strains
$\{\varepsilon_x\ \varepsilon_y\ \varepsilon_z\ \gamma_{xy}\ \gamma_{yz}\ \gamma_{xz}\}^T$	global strain vector
$\{\varepsilon_1\ \varepsilon_2\ \varepsilon_3\ \gamma_{12}\ \gamma_{23}\ \gamma_{13}\}^T$	biaxial principal strains in 1–2–3 direction
$\{\bar{\varepsilon}_1\ \bar{\varepsilon}_2\ \bar{\varepsilon}_3\}^T$	equivalent uniaxial strains
ε_{1p}, ε_{2p}, ε_{3p}	ultimate strain in 1–2–3 directions
$\bar{\varepsilon}_{sx}$, $\bar{\varepsilon}_{sy}$, $\bar{\varepsilon}_{sz}$	equivalent uniaxial strain in the reinforcement in x, y and z directions
$\{\mu_{12}\ \mu_{21}\ \mu_{23}\ \mu_{32}\ \mu_{13}\ \mu_{31}\}^T$	Hsu/Zhu ratios
ζ	softened coefficient of concrete in compression
ρ_{sx}, ρ_{sy}, ρ_{sz}	smeared steel ratio in x, y and z directions
$\{\sigma\} = \{\sigma_x\ \tau_{xy}\ \tau_{xz}\}^T$	available stresses
$\{\sigma_x\ \sigma_y\ \sigma_z\ \tau_{xy}\ \tau_{yz}\ \tau_{xz}\}^T$	global total stress vector
σ_{1p}, σ_{2p}, σ_{3p}	ultimate stresses in 1–2–3 directions
$\{\sigma^c_1\ \sigma^c_2\ \sigma^c_3\ \tau^c_{12}\ \tau^c_{23}\ \tau^c_{13}\}^T$	local concrete stress vector in 1–2–3 direction

Introduction

Reinforced concrete (RC) structural walls are effective in resisting lateral loads imposed on buildings. They provide substantial strength as well as the deformation capacity needed to meet the demands of severe loading conditions. Simulation of the complex behaviour of RC shear walls requires accurate constitutive modelling of the RC material. Two-dimensional (2D) continuum plane stress or three-dimensional (3D) solid elements are typically used for this purpose, but such elements are computationally very expensive. Previous studies showed that beam–column elements can be used to simulate the behaviour of RC shear walls (Bolander and Wight, 1991). Care needs to be

exercised, however, when using such elements since they cannot simulate localised damage and local distortions in detailed regions such as near openings. In addition, beam–column elements based on elementary beam theories cannot predict the behaviour of walls with small aspect ratios, typically less than 1 (Mazars *et al.*, 2002).

Fibre beam–column elements (Spacone *et al.*, 1996) are considered the most efficient beam elements owing to their ability to accurately describe section behaviour through fibre discretisation. Recently, these elements were extended in the context of a Timoshenko beam formulation to consider shear effects (Mullapudi, 2010; Mullapudi and Ayoub, 2010). Such elements permit accurate evaluation of the behaviour of walls dominated by shear as well as flexural behaviour, and are computationally suitable to conduct parameter studies to investigate the effect of the different parameters affecting the wall behaviour.

Lefas and Kotsovos (1990) analysed shear walls under monotonically increasing lateral loads. The authors used eight node isoparametric elements to model concrete and a three node bar to model steel. Steel bars coincided with the sides of adjacent concrete elements. Orakcal and Wallace (2006) presented detailed information on the calibration of a non-linear wall macro model by comparing model results with experimental results for slender RC walls with T-shaped and rectangular cross sections. Results obtained with the analytical model for rectangular walls agree with experimental responses for flexural capacity, stiffness and deformability, although some significant variations are noted in local compression strains.

Peng and Wong (2011) recently conducted experiments on RC shear walls under monotonic eccentric lateral load with different torque to moment ratios. The authors found that the flexural strength and ductility were significantly reduced in the presence of torque.

In the past three decades, constitutive models describing the behaviour of concrete have considerably progressed, thereby improving the numerical performance of RC structures. The constitutive laws of concrete and steel bars are typically developed and calibrated through large-scale panel testing and relate the smeared stresses to the smeared strains of the element (Hsu *et al.*, 1995).

An RC element under combined loading is a complex problem owing to the presence of normal and shear stresses, in addition to the shear caused by torsion. Vecchio and Selby (1991) developed a finite-element program for 3D analysis of RC structures using an eight node regular hexahedral element. Their constitutive material model employed the modified compression field theory. Cocchi and Volpi (1996) presented a non-linear analysis of RC members subjected to combined axial, shear, bending and torsional loads, based on an extension of the diagonal compression field theory. It is assumed that after concrete cracks under torsion, the member becomes a hollow section with varying wall thickness; shear deformations are not considered in the formulation. Bairan and Mari (2006, 2007) developed a non-linear 3D sectional model to account for combined loadings including torsion, with a 3D constitutive model that allows warping and sections shape distortion. They considered the coupled model for arbitrary shaped cross-sections made of heterogeneous anisotropic materials under 3D combined loadings. The theory is based on equilibrium considerations and the superposition of 3D section distortion as well as plane section hypothesis. Gregori *et al.* (2007) developed a 3D model subjected to combined loading conditions including axial, bending, shear and torsional loads. The proposed fibre beam–column element model is a displacement-based Timoshenko beam with simple kinematic assumptions.

To predict the complete pre- and post-peak responses of the shear stress–strain curves, the softened membrane model (SMM) is adopted in this study, along with the Hsu/Zhu ratio (Poisson ratio of cracked RC). The study tackles the extension of the fibre-based beam element formulation to account for axial, bending, shear and torsion interaction. Such interaction is essential to predict accurately the complex behaviour of RC wall members under combined loads. The model is developed using the finite-element program FEAPpv (Taylor, 2005). The fibre beam–column formulation for shear-critical elements is presented first.

Displacement-based formulation

The model is developed based on a Timoshenko-type displacement formulation with the assumption that plane sections remain plane. The element comprises a two node frame member that follows a directrix line between nodes one and two (Figure 1). Each element is divided into several sections along the length of the element and into several fibres across the cross section of the member. The strain in each fibre is calculated from the centroidal section strain and curvature with the help of the plane section remaining plane assumption. The stresses and modulus of fibres are calculated from the fibre strain values. The constitutive relation of the section is derived by integration of the response of the fibres; and the response of the element is also derived by integration of the response of sections along the length of the element.

The 3D response is described by defining six degrees of freedom at each section of the element, which consists of three translations u_0, v_0, w_0 and three rotations θ_x, θ_y, θ_z with the corresponding forces N, V, W and moments T, M_y, M_z, respectively.

The kinematic assumptions are used to relate the displacements at any point with the element degrees of freedom according to the following equations

$$1. \quad u(x, y, z) = u_0(x) + z\theta_y(x) - y\theta_z(x)$$

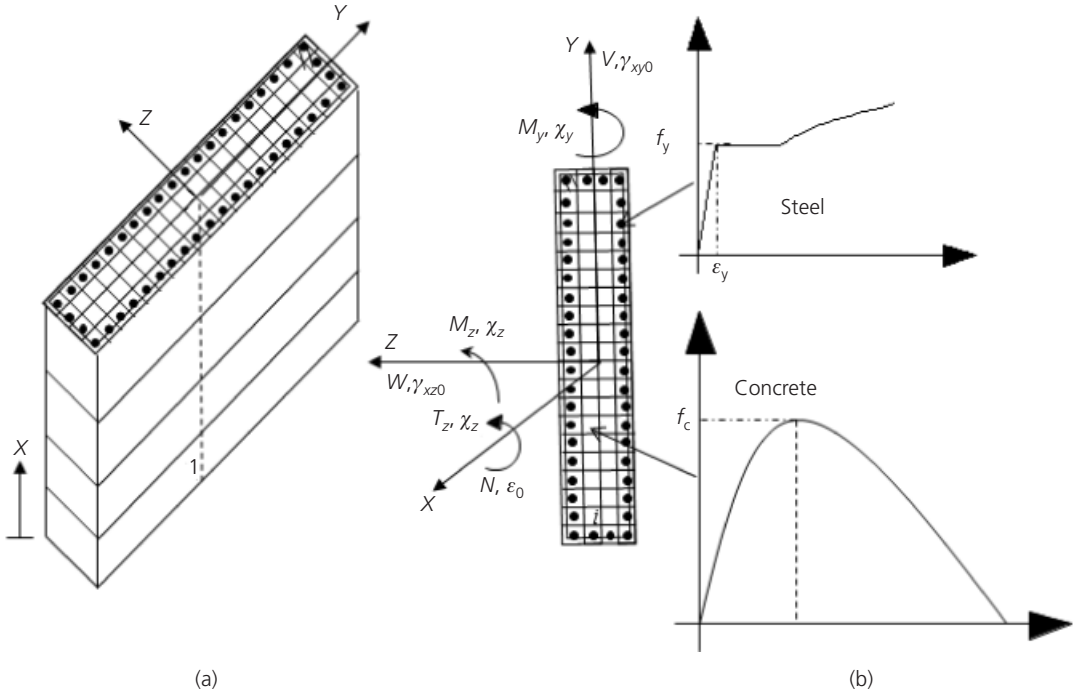

Figure 1. (a) Wall element; (b) wall fibre discretisation

2. $$v(x,\ y,\ z) = v_0(x) - z\theta_x(x)$$

3. $$w(x,\ y,\ z) = w_0(x) + y\theta_x(x)$$

Each element is further divided into a number of sections composed of integration points. Section deformations and forces are related to element deformations (Figure 2(a)) and forces (Figure 2(b)) according to the given displacement shape functions.

Equations 4–6 are used to derive the three strain components ε_x, γ_{xy} and γ_{xz} at every section of the element

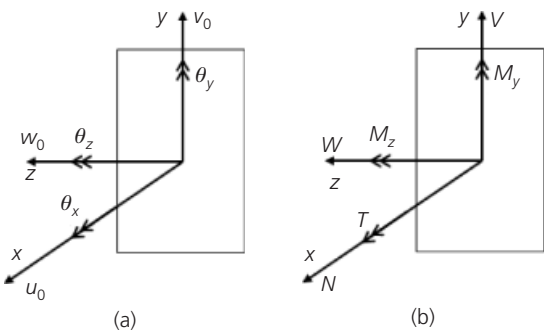

Figure 2. (a) Section displacements; (b) section forces

4. $$\varepsilon_x = \frac{\partial u}{\partial x} = \frac{\partial u_0}{\partial x} + z\frac{\partial \theta_y}{\partial x} - y\frac{\partial \theta_z}{\partial x}$$

5. $$\gamma_{xy} = \frac{\partial u}{\partial y} + \frac{\partial v}{\partial x} = \left(\frac{\partial v_0}{\partial x} - \theta_z\right) - z\frac{\partial \theta_x}{\partial x}$$

6. $$\gamma_{xz} = \frac{\partial u}{\partial z} + \frac{\partial w}{\partial x} = \left(\frac{\partial w_0}{\partial x} + \theta_y\right) + y\frac{\partial \theta_x}{\partial x}$$

where ε_x is the normal strain and γ_{xy} and γ_{xz} are the shear strains. The remaining strain vectors ε_y, ε_z and γ_{yz} are determined by enforcing equilibrium between the concrete and the steel, satisfying the equations $\sigma_y = 0$, $\sigma_z = 0$ and $\tau_{yz} = 0$.

The available strains ε and corresponding stresses σ can be written in vector form as

7. $$\{\varepsilon\} = \left\{\varepsilon_x \quad \gamma_{xy} \quad \gamma_{xz}\right\}^T;$$
$$\{\sigma\} = \left\{\sigma_x \quad \tau_{xy} \quad \tau_{xz}\right\}^T$$

Section deformations at the centre of the section, in matrix form, can be written as

$$\{s\} = \left\{ \varepsilon_0 \;\; \chi_y \;\; \chi_z \;\; \chi_x \;\; \gamma_{xy0} \;\; \gamma_{xz0} \right\}^T$$

$$= \left\{ \frac{\partial u_0}{\partial x} \;\; \frac{\partial \theta_y}{\partial x} \;\; -\frac{\theta_z}{\partial x} \;\; \frac{\partial \theta_x}{\partial x} \;\; \frac{\partial v_0}{\partial x} - \theta_z \;\; \frac{\partial w_0}{\partial x} + \theta_y \right\}^T \quad (8)$$

The strain vector at the fibre level ε is related to the sectional strain s as follows

$$\{\varepsilon\} = \left\{ \varepsilon_x \quad \gamma_{xy} \quad \gamma_{xz} \right\}^T = [T]\{s\} \quad (9)$$

$$[T] = \begin{bmatrix} 1 & z & y & 0 & 0 & 0 \\ 0 & 0 & 0 & -z & 1 & 0 \\ 0 & 0 & 0 & y & 0 & 1 \end{bmatrix} \quad (10)$$

where ε_0 is the longitudinal strain at the section centroid, χ_y and χ_z are the curvatures about the y- and z- coordinate system, χ_x is the angle of twist per unit length, and γ_{xy0} and γ_{xz0} are the generalised shear strains.

The weak form of the displacement formulation is based on the principal of virtual work and is demonstrated by the following equation

$$\iint_\Omega \delta\varepsilon^T \sigma \, \mathrm{d}\Omega = \iint_\Omega \delta s^T T^T \sigma \, \mathrm{d}\Omega$$

$$= \delta s^T \iint_\Omega T^T \sigma \, \mathrm{d}\Omega = \delta s^T F \quad (11)$$

where F is the resulting sectional force vector

$$F = \iint_\Omega T^T \sigma \, \mathrm{d}\Omega = \iint_\Omega T^T \sigma \, \mathrm{d}\Omega = \iint_\Omega T^T \sigma \, \mathrm{d}\Omega$$

$$= \iint_\Omega \begin{bmatrix} 1 & z & y & 0 & 0 & 0 \\ 0 & 0 & 0 & -z & 1 & 0 \\ 0 & 0 & 0 & y & 0 & 1 \end{bmatrix}^T \begin{Bmatrix} \sigma_x \\ \tau_{xy} \\ \tau_{xz} \end{Bmatrix} \mathrm{d}\Omega$$

$$= [N \quad M_y \quad M_z \quad T \quad V_y \quad V_z] \quad (12)$$

The tangent stiffness of the section is calculated as

$$[K_{\text{section}}] = \frac{\{\partial F\}}{\{\partial \varepsilon\}} = \iint_\Omega \frac{\partial}{\partial \varepsilon} (T^T \sigma) \mathrm{d}\Omega$$

$$= \iint_\Omega T^T \frac{\partial \sigma}{\partial \varepsilon} \mathrm{d}\Omega$$

$$= \iint_\Omega T^T \frac{\partial \sigma}{\partial s} \frac{\partial s}{\partial \varepsilon} \mathrm{d}\Omega = \iint_\Omega T^T D_{\text{gl}} T \, \mathrm{d}\Omega \quad (13)$$

The nodal displacements at each integration point or section are derived from the elemental end node displacements as $\{u\} = [a]\{d\}$

$$\{u\} = \begin{Bmatrix} u \\ v \\ w \\ \theta_x \\ \theta_y \\ \theta_z \end{Bmatrix}_{6\times 1} = \begin{bmatrix} N_1 & 0 & 0 & 0 & 0 & 0 & N_2 & 0 & 0 & 0 & 0 & 0 \\ 0 & N_1 & 0 & 0 & 0 & 0 & 0 & N_2 & 0 & 0 & 0 & 0 \\ 0 & 0 & N_1 & 0 & 0 & 0 & 0 & 0 & N_2 & 0 & 0 & 0 \\ 0 & 0 & 0 & N_1 & 0 & 0 & 0 & 0 & 0 & N_2 & 0 & 0 \\ 0 & 0 & 0 & 0 & N_1 & 0 & 0 & 0 & 0 & 0 & N_2 & 0 \\ 0 & 0 & 0 & 0 & 0 & N_1 & 0 & 0 & 0 & 0 & 0 & N_2 \end{bmatrix}_{6\times 6n} \begin{Bmatrix} u_1 \\ v_1 \\ w_1 \\ \theta_{x1} \\ \theta_{y1} \\ \theta_{z1} \\ u_2 \\ v_2 \\ w_2 \\ \theta_{x2} \\ \theta_{y2} \\ \theta_{z2} \end{Bmatrix}_{6n\times 1} \quad (14)$$

where n is the number of nodes of the element.

The section strains vector $\{s\} = [B]\{d\}$ derived from nodal displacements is given by

$$15.\quad \begin{Bmatrix} \varepsilon_0 \\ \chi_y \\ \chi_z \\ \chi_x \\ \gamma_{xy0} \\ \gamma_{xz0} \end{Bmatrix} = \begin{bmatrix} N_{1,x} & 0 & 0 & 0 & 0 & 0 & N_{2,x} & 0 & 0 & 0 & 0 & 0 \\ 0 & 0 & 0 & 0 & N_{1,x} & 0 & 0 & 0 & 0 & 0 & N_{2,x} & 0 \\ 0 & 0 & 0 & 0 & 0 & -N_{1,x} & 0 & 0 & 0 & 0 & 0 & -N_{2,x} \\ 0 & 0 & 0 & N_{1,x} & 0 & 0 & 0 & 0 & 0 & N_{2,x} & 0 & 0 \\ 0 & N_{1,x} & 0 & 0 & 0 & -N_1 & 0 & N_{2,x} & 0 & 0 & 0 & -N_2 \\ 0 & 0 & N_{1,x} & 0 & N_1 & 0 & 0 & 0 & N_{2,x} & 0 & N_2 & 0 \end{bmatrix} \begin{Bmatrix} u_1 \\ v_1 \\ w_1 \\ \theta_{x1} \\ \theta_{y1} \\ \theta_{z1} \\ u_2 \\ v_2 \\ w_2 \\ \theta_{x2} \\ \theta_{y2} \\ \theta_{z2} \end{Bmatrix}$$

The exact integration of the Timoshenko beam formulation using linear shape functions produces parasitic shear; this leads to a solution that is too stiff, which results in a slow convergence rate owing to shear locking. This problem can be solved by using reduced integration schemes, such as a one-point integration rule. Unfortunately, in this case, the solution depends on the integration point.

In the calculation of shear strains, the section rotations θ_y and θ_z are linear in x, and $\frac{\partial v}{\partial x}$ and $\frac{\partial w}{\partial x}$ are constant in x, which leads to shear locking. This problem can be solved by assuming a linear shear strain distribution through the use of a linear shape function for rotations and a quadratic shape function for deflections (Mullapudi and Ayoub, 2009).

In this case, the deflection or transverse displacement in quadratic terms can be written as

$$16.\quad v(x) = \frac{L-x}{L}v_1 + \frac{x}{L}v_2 + \frac{x(L-x)}{2L}(\theta_{z1} - \theta_{z2})$$

$$17.\quad w(x) = \frac{L-x}{L}w_1 + \frac{x}{L}w_2 + \frac{x(L-x)}{2L}(\theta_{y1} - \theta_{y2})$$

where L is the length of the element.

The rotation in linear terms can be written as

$$18.\quad \theta_y(x) = \frac{L-x}{L}\theta_{y1} + \frac{x}{L}\theta_{y2}$$

$$19.\quad \theta_z(x) = \frac{L-x}{L}\theta_{z1} + \frac{x}{L}\theta_{z2}$$

The element stiffness can be calculated from the section stiffness using

$$20.\quad [K_{\text{element}}] = \iint_A B^T K_{\text{section}} B \mathrm{d}A$$

The resisting load $\{R\}$ is calculated from the section forces using

$$21.\quad \{R\} = \iint_A B^T F \mathrm{d}A$$

The finite-element solution for a displacement increment Δd can be calculated from

$$22.\quad K_{\text{element}} \Delta d = \Delta R$$

The section behaviour, as stated earlier, is evaluated through fibre discretisation with the appropriate material constitutive models. Longitudinal steel fibres are assumed to follow a smeared stress–strain relation.

Concrete constitutive model

The 3D regions have six stresses $\{\sigma_{3D}\}$ and corresponding strains $\{\varepsilon_{3D}\}$; however, the current beam formulation considers only three stress $\{\sigma\}$ and strain $\{\varepsilon\}$ components, while the other three stress and strain components are derived by solving the given equilibrium conditions

$$23.\quad \{\sigma_{3D}\} = \{\sigma_x \quad \sigma_y \quad \sigma_z \quad \tau_{xy} \quad \tau_{yz} \quad \tau_{xz}\}^T$$
$$\{\varepsilon_{3D}\} = \{\varepsilon_x \quad \varepsilon_y \quad \varepsilon_z \quad \gamma_{xy} \quad \gamma_{yz} \quad \gamma_{xz}\}^T$$

$$\{\sigma\} = \begin{bmatrix} \sigma_x & \tau_{xy} & \tau_{xz} \end{bmatrix}^T$$

$$\{\varepsilon\} = \begin{bmatrix} \varepsilon_x & \varepsilon_y & \gamma_{xz} \end{bmatrix}^T \quad (24)$$

$$\{\sigma_{UN}\} = \begin{bmatrix} \sigma_y & \sigma_z & \tau_{yz} \end{bmatrix}^T$$

$$\{\varepsilon_{UN}\} = \begin{bmatrix} \varepsilon_y & \varepsilon_z & \gamma_{yz} \end{bmatrix}^T \quad (25)$$

The unknown stress components σ_{UN} should be 0 to satisfy the internal equilibrium between the reinforcing steel and concrete, which will result in the corresponding three unknown strain values ε_{UN}. As the constraint condition is non-linear, determination of the corresponding strains requires an iterative solution. The proposed algorithm is shown in Figure 3 and is described in detail in Mullapudi (2010).

The eigen vectors, or direction cosines $[\alpha_1]$ used in Figure 3 to determine the principal directions from the applied stresses σ_{3D} are

$$[\alpha_1] = \begin{bmatrix} l_1 & l_2 & l_3 \\ m_1 & m_2 & m_3 \\ n_1 & n_2 & n_3 \end{bmatrix} \quad (26)$$

To rotate the stress and strain vectors from the global x–y–z system to the applied principal stress direction system 1–2–3 with an angle of $[\alpha_1]$, the rotation matrix R is used

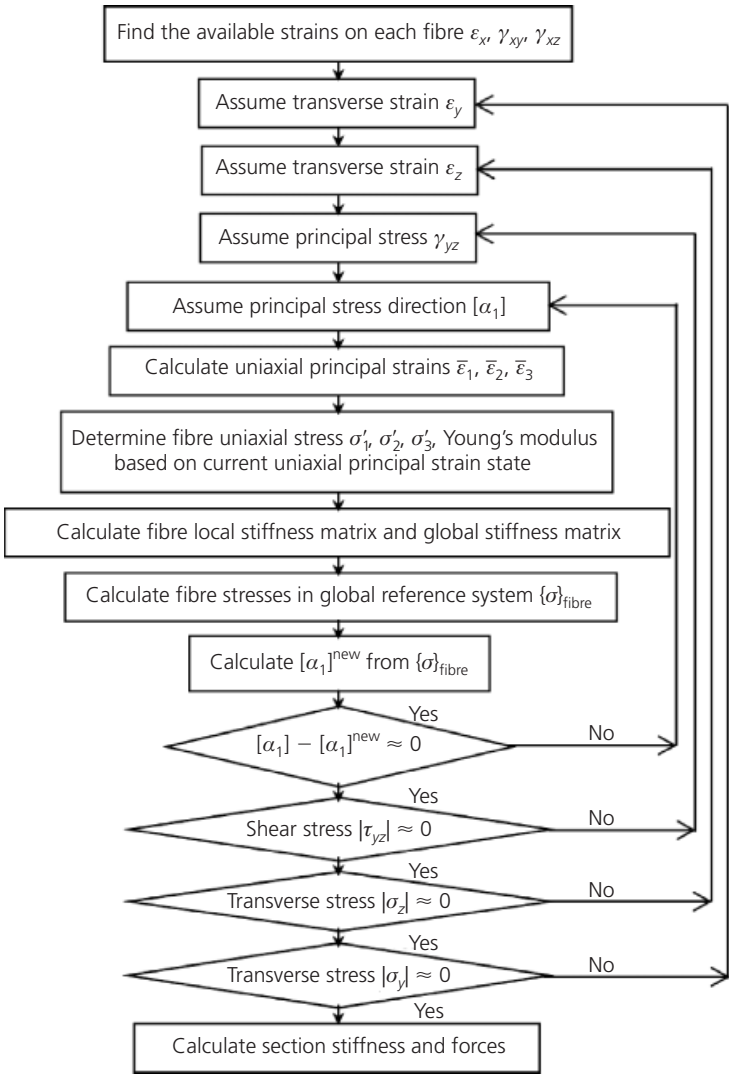

Figure 3. Iterative procedure to determine required 3D strains

$$[R(\alpha_1)] = \begin{bmatrix} l_1^2 & m_1^2 & n_1^2 & l_1 m_1 & m_1 n_1 & n_1 l_1 \\ l_2^2 & m_2^2 & n_2^2 & l_2 m_2 & m_2 n_2 & n_2 l_2 \\ l_3^2 & m_3^2 & n_3^2 & l_3 m_3 & m_3 n_3 & n_3 l_3 \\ 2l_1 l_2 & 2m_1 m_2 & 2n_1 n_2 & l_1 m_2 + l_2 m_1 & m_1 n_2 + m_2 n_1 & n_1 l_2 + n_2 l_1 \\ 2l_2 l_3 & 2m_2 m_3 & 2n_2 n_3 & l_2 m_3 + l_3 m_2 & m_2 n_3 + m_3 n_2 & n_2 l_3 + n_3 l_2 \\ 2l_3 l_1 & 2m_3 m_1 & 2n_3 n_1 & l_3 m_1 + l_1 m_3 & m_3 n_1 + m_1 n_3 & n_3 l_1 + n_1 l_3 \end{bmatrix} \quad (27)$$

In a fibre-based element formulation, the process of the state determination at the fibre level requires the calculation of the fibre stresses $[\sigma_x \ \sigma_y \ \sigma_z \ \tau_{xy} \ \tau_{yz} \ \tau_{xz}]^T$ from the strain state $[\varepsilon_x \ \varepsilon_y \ \varepsilon_z \ \gamma_{xy} \ \gamma_{yz} \ \gamma_{xz}]^T$. Because the model has been implemented in a Timoshenko-type beam formulation, the values of ε_x, γ_{xy} and γ_{xz} are typically known, while the lateral strains ε_y and ε_z values must be evaluated from the equilibrium.

Evaluation of lateral strain

The equilibrium equations needed to evaluate the stresses in the x–y–z coordinate system $[\sigma_x \ \sigma_y \ \sigma_z \ \tau_{xy} \ \tau_{yz} \ \tau_{xz}]^T$ as a function of the principal stresses resisted by concrete $[\sigma_1^c \ \sigma_2^c \ \sigma_3^c \ \tau_{12}^c \ \tau_{23}^c \ \tau_{13}^c]^T$ and the reinforcing bar stresses f_{sx}, f_{sy} and f_{sz} along the x, y and z directions, respectively, are

$$\begin{aligned} &\{\sigma_x \quad \sigma_y \quad \sigma_z \quad \tau_{xy} \quad \tau_{yz} \quad \tau_{xz}\}^T \\ &\quad = [R(\alpha_1)]^{-1}\{\sigma_1^c \quad \sigma_2^c \quad \sigma_3^c \quad \tau_{12}^c \quad \tau_{23}^c \quad \tau_{13}^c\}^T \\ &\quad + \{\rho_{sx} f_{sx} \quad \rho_{sy} f_{sy} \quad \rho_{sz} f_{sz} \quad 0 \quad 0 \quad 0\}^T \end{aligned} \quad (28)$$

where $[R]$ is the rotation matrix, $[R]^{-1} = [R]^T$, and ρ_{sx}, ρ_{sy} and ρ_{sz} are the smeared reinforcement ratios in the x, y and z directions, respectively.

Transverse strains are internal variables determined by imposing equilibrium on each fibre between concrete and steel stirrups. Stirrup strains are not known in advance, and because of the non-linear behaviour of the concrete and steel, an iterative procedure is needed to satisfy the equilibrium in the y and z directions, following the flow chart in Figure 3.

The second of the equilibrium equations in Equation 28 is used to evaluate the lateral strain ε_y in fibre i, taking into consideration that the value of σ_y equals 0

$$\begin{aligned} &\sigma_1^{c,i} m_1^2 + \sigma_2^{c,i} m_2^2 + \sigma_3^{c,i} m_3^2 + \tau_{12}^{c,i} 2m_1 m_2 \\ &+ \tau_{23}^{c,i} 2m_2 m_3 + \tau_{31}^{c,i} 2m_1 m_3 + \rho_{sy}^i f_{sy}^i = 0 \end{aligned} \quad (29)$$

The third of the equilibrium equations in Equation 28 is used to evaluate the lateral strain ε_z in fibre i; taking into consideration that the value of σ_z equals 0

$$\begin{aligned} &\sigma_1^{c,i} n_1^2 + \sigma_2^{c,i} n_2^2 + \sigma_3^{c,i} n_3^2 + \tau_{12}^{c,i} 2n_1 n_2 \\ &+ \tau_{23}^{c,i} 2n_2 n_3 + \tau_{31}^{c,i} 2n_3 n_1 + \rho_{sz}^i f_{sz}^i = 0 \end{aligned} \quad (30)$$

Here, ρ_{sy}^i, ρ_{sz}^i are the ratios of steel to concrete area in the y and z directions of fibre i, and f_{sy}^i, f_{sz}^i are the transverse steel bar stresses in the y and z directions of fibre i.

An iterative procedure is needed to determine the lateral strain ε_y and ε_z that will also satisfy the previous two equations because of the non-linear behaviour of the concrete and steel. An initial value for ε_y and ε_z is assumed at each fibre, and the iterations proceed until Equations 29 and 30 are internally satisfied.

Evaluation of concrete stress

The typical concrete stress–strain curves are derived from uniaxial tests, so the biaxial strains in the x–y–z direction $[\varepsilon_x \ \varepsilon_y \ \varepsilon_z \ \gamma_{xy} \ \gamma_{yz} \ \gamma_{xz}]^T$ need to be converted to equivalent uniaxial strains in the 1–2–3 direction $[\bar{\varepsilon}_1 \ \bar{\varepsilon}_2 \ \bar{\varepsilon}_3 \ \gamma_{12} \ \gamma_{23} \ \gamma_{13}]^T$ to calculate the concrete stresses.

The direction of cracks is first calculated based on the strain state. At this angle, the concrete shear stresses τ_{12}^c, τ_{23}^c and τ_{13}^c become 0, and the corresponding constitutive model becomes a rotating angle softened truss model. The calculated principal angle $[\alpha_1]$ from the known stress state is evaluated after the ε_y, ε_z and γ_{yz} terms that satisfy the equilibrium conditions are determined.

The biaxial principal strains are then evaluated as

$$\begin{aligned} &\{\varepsilon_1 \quad \varepsilon_2 \quad \varepsilon_3 \quad \gamma_{12} \quad \gamma_{23} \quad \gamma_{13}\}^T \\ &\quad = [R(\alpha_1)]\{\varepsilon_x \quad \varepsilon_y \quad \varepsilon_z \quad \gamma_{xy} \quad \gamma_{yz} \quad \gamma_{xz}\}^T \end{aligned} \quad (31)$$

Biaxial principal strains are needed to evaluate the equivalent uniaxial strains. The equivalent uniaxial strains are derived from the biaxial strains with the help of the suggested Poisson ratio of cracked concrete, also called the Hsu/Zhu ratios $\{\mu_{12} \ \mu_{21} \ \mu_{23} \ \mu_{32} \ \mu_{13} \ \mu_{31}\}^T$ (Zhu and Hsu, 2002). From the range of $j = 1$ to 3 and $k = 1$ to 3, μ_{jk} is the ratio of the resulting tensile strain increment in the principal j direction to the source compressive strain increment in the principal k direction; μ_{kj} is the ratio of the resulting compressive strain increment in the

principal k direction to the tensile source strain increment in the principal j direction. The following equations are suggested by Jeng and Hsu (2009) for members subjected to torsion

$$\mu_{jk} = 0{\cdot}16 + 680\varepsilon_{sf},\ \varepsilon_{sf} \leqslant \varepsilon_{yd} \tag{32}$$

$$\mu_{jk} = 1{\cdot}52,\ \varepsilon_{sf} > \varepsilon_{yd} \tag{33}$$

$$\mu_{kj} = 0 \tag{34}$$

where ε_{sf} is defined as the strain in the reinforcement that yields first, and ε_{yd} is the yield strain of reinforcing steel.

After cracking, the Hsu/Zhu ratio μ_{jk} lies outside the typical range of 0 to 0·5 for the Poisson ratio of continuous materials; before cracking the Hsu/Zhu ratio $\mu_{kj} = 0{\cdot}2$; and after cracking the Hsu/Zhu ratio $\mu_{kj} = 0$, indicating that the tensile strain has no effect on the compressive strain.

The equivalent uniaxial strains are derived from the biaxial principal strains with Hsu/Zhu ratios $\{\mu_{12}\ \mu_{21}\ \mu_{23}\ \mu_{32}\ \mu_{13}\ \mu_{31}\}^T$ as

$$\left\{\begin{array}{ccc}\overline{\varepsilon}_1 & \overline{\varepsilon}_2 & \overline{\varepsilon}_3\end{array}\right\}^T = [\mu]\left\{\begin{array}{ccc}\varepsilon_1 & \varepsilon_2 & \varepsilon_3\end{array}\right\}^T \tag{35}$$

where

$$[\mu] = \begin{bmatrix} 1 & -\mu_{12} & -\mu_{13} \\ -\mu_{21} & 1 & -\mu_{23} \\ -\mu_{31} & -\mu_{32} & 1 \end{bmatrix}^{-1} \tag{36}$$

The equivalent uniaxial strain in the longitudinal and transverse reinforcement is derived after evaluating the direction cosines $[\alpha_1]$ and the rotation matrix $[R(\alpha_1)]$.

The equivalent uniaxial strain in the longitudinal reinforcement along the x direction with the effect of the Hsu/Zhu ratio is given by

$$\overline{\varepsilon}_{sx} = \overline{\varepsilon}_1 l_1^2 + \overline{\varepsilon}_2 l_2^2 + \overline{\varepsilon}_3 l_3^2 + \gamma_{12} 2 l_1 l_2 + \gamma_{23} 2 l_2 l_3 + \gamma_{13} 2 l_1 l_3 \tag{37}$$

The equivalent uniaxial strain in the transverse reinforcement along the y direction with the effect of the Hsu/Zhu ratio is given by

$$\overline{\varepsilon}_{sy} = \overline{\varepsilon}_1 m_1^2 + \overline{\varepsilon}_2 m_2^2 + \overline{\varepsilon}_3 m_3^2 + \gamma_{12} 2 m_1 m_2 + \gamma_{23} 2 m_2 m_3 + \gamma_{13} 2 m_1 m_3 \tag{38}$$

The equivalent uniaxial strain in the transverse reinforcement along the z direction with the effect of the Hsu/Zhu ratio is given by

$$\overline{\varepsilon}_{sz} = \overline{\varepsilon}_1 n_1^2 + \overline{\varepsilon}_2 n_2^2 + \overline{\varepsilon}_3 n_3^2 + \gamma_{12} 2 n_1 n_2 + \gamma_{23} 2 n_2 n_3 + \gamma_{13} 2 n_1 n_3 \tag{39}$$

The equivalent uniaxial longitudinal steel stress f_{sx}, transverse steel stresses f_{sy} and f_{sz} are calculated from the equivalent uniaxial steel reinforcement strains $\overline{\varepsilon}_{sx}$, $\overline{\varepsilon}_{sy}$ and $\overline{\varepsilon}_{sz}$ through a bi-linear stress–strain relationship (Belarbi and Hsu, 1994, 1995).

The current equivalent uniaxial strains $\overline{\varepsilon}_1$, $\overline{\varepsilon}_2$ and $\overline{\varepsilon}_3$ are individually used to calculate the concrete stresses σ_1^c, σ_2^c and σ_3^c in the principal direction of the uniaxial concrete material stress–strain relationship. The concrete constitutive relations are described in more detail in the next section.

Concrete triaxial constitutive relations

The concrete constitutive equations depend on the strain state and the region of the cross section. The principal strains ε_1, ε_2 and ε_3 are found from the global strains using the iterative algorithm of Figure 3 and the Jacobi method; and the equivalent uniaxial strains $\overline{\varepsilon}_1$, $\overline{\varepsilon}_2$ and $\overline{\varepsilon}_3$ are derived based on the Hsu/Zhu ratio (Jeng and Hsu, 2009). The local concrete material stiffness is derived based on Young's modulus and the Hsu/Zhu ratio. The global stiffness in the Cartesian direction is calculated by transforming the local stiffness to the global direction. The global stiffness in the y, z and yz directions are condensed in the element formulation and, during this process, the stresses in the axial, flexure and shear directions are coupled.

The values of the concrete uniaxial strains in principal directions 1, 2 and 3 have eight conditions, and the strength in one direction is affected by the strain state in the other directions following the procedure proposed by Vecchio and Selby (1991). The uniaxial strains are sorted in ascending order such that $\overline{\varepsilon}_1 > \overline{\varepsilon}_2 > \overline{\varepsilon}_3$. The values of concrete compressive strength σ_1^c in direction 1 and concrete compressive strength σ_3^c in direction 3 can be found based on their strain state, as discussed next. The same type of rules applies for the 1–2 direction to determine the concrete compressive strength σ_2^c in direction 2.

Case 1: 1–tension, 3–compression

In case 1, the equivalent uniaxial strain of concrete $\overline{\varepsilon}_1$ in principal direction 1 is in tension, and the equivalent uniaxial strain $\overline{\varepsilon}_3$ in principal direction 3 is in compression. The uniaxial concrete stress σ_1^c in direction 1 is calculated from $\overline{\varepsilon}_1$ and is not a function

of the perpendicular concrete strain $\bar{\varepsilon}_3$. The compressive strength in principal direction 3, σ_3^c, will however, soften because of the tension in the orthogonal direction. Jeng and Hsu (2009) derived a softening equation in the tension–compression region, which is implemented in the current model, and is based on panel testing, as proposed by Hsu and Zhu (2002). The equation for the compressive strength and strain reduction factor ζ is given by

$$\zeta = \left(\frac{5{\cdot}8}{\sqrt{f'_c(\text{MPa})}} \leqslant 0{\cdot}9\right) \times \left(\frac{1}{\sqrt{1+400\bar{\varepsilon}_1}}\right)\left(1-\frac{|\alpha^*_{r1}|}{32^\circ}\right) \quad (40)$$

where

$$\alpha^*_{r1} = 0{\cdot}5\tan^{-1}\left(\frac{2\gamma_{13}}{\varepsilon_1-\varepsilon_3}\right) \quad (41)$$

The softening coefficient ζ value is limited to 0·9 because the uniaxial concrete compressive strength f'_c is calculated from standard cylinder tests, while results of panel experiments performed at the University of Houston showed that the concrete strength does not reach f'_c. These results are attributable to the panel size and shape, and loading rate, which have ample effect on the concrete compressive strength f'_c. The ultimate stress in the orthogonal direction is $\zeta f'_c$ at softened strain $\zeta\varepsilon_0$ when ζ is the softening coefficient; α^*_{r1} is the deviation angle in degrees, which is the difference between the applied stress angle α_1 and the rotating angle through global strain values; $\bar{\varepsilon}_1$ is the lateral tensile strain; ε_0 is the concrete strain at peak compressive strength f'_c; and $\zeta f'_c$ is the softened concrete compressive strength.

Case 2: 1–tension, 3–tension

The equivalent uniaxial strain of concrete $\bar{\varepsilon}_1$ in direction 1 is in tension, and the equivalent uniaxial strain $\bar{\varepsilon}_3$ of concrete in direction 3 is also in tension. In case 2, the uniaxial concrete stress σ_1^c in direction 1 is evaluated from $\bar{\varepsilon}_1$, and σ_2^c in direction 3 is evaluated from $\bar{\varepsilon}_3$. σ_1^c and σ_3^c are functions only of the orthogonal concrete strains $\bar{\varepsilon}_1$ and $\bar{\varepsilon}_3$, respectively.

Case 3: 1–compression, 3–compression

The equivalent uniaxial strains of concrete in principal directions 1 and 3 are in compression. The current research uses the Vecchio (1992) simplified version of the Kupfer *et al.* (1969) biaxial compression strength equation. The concrete compressive strength increase in one direction depends on the confining stress in the orthogonal direction. The enhanced strength and increased ductility depend on the biaxial compressive stresses. Concrete in compression exhibits lateral expansion and increases in the value of the Poisson ratio. An upper limit of 0·5 has been set for the Poisson ratio. The principal stresses in the two orthogonal directions are denoted by σ_1^c, σ_3^c, and their corresponding strains are referred to by the functions $\bar{\varepsilon}_1$ and $\bar{\varepsilon}_3$. The equations for the biaxial compression failure surface are

$$K_{c1} = 1 + 0{\cdot}92\left(\frac{-\sigma_3^c}{f'_c}\right) - 0{\cdot}76\left(\frac{-\sigma_3^c}{f'_c}\right)^2$$

$$K_{c3} = 1 + 0{\cdot}92\left(\frac{-\sigma_1^c}{f'_c}\right) - 0{\cdot}76\left(\frac{-\sigma_1^c}{f'_c}\right)^2 \quad (42)$$

where K_{c1} and K_{c3} are the biaxial strength magnification factors. The ultimate stresses in the orthogonal directions are

$$\sigma_{1p} = K_{c1}f'_c, \quad \sigma_{3p} = K_{c3}f'_c \quad (43)$$

The ultimate strains in the orthogonal directions are

$$\varepsilon_{1p} = K_{c1}\varepsilon_0, \quad \varepsilon_{3p} = K_{c3}\varepsilon_0 \quad (44)$$

where ε_0 is the uniaxial compressive strain of the concrete at peak stress.

Analysis of shear walls

RC shear walls are typically modelled with 2D continuum elements or 3D solid elements. Such models can accurately describe the local behaviour of the wall element. Continuum and solid models are computationally very expensive though, which limits their applicability to larger structures. Fibre beam elements, on the other hand, are able to model the behaviour of slender walls and are computationally efficient. With the inclusion of shear deformations and concrete constitutive models under a biaxial state of stress, fibre models can also accurately simulate the behaviour of walls with aspect ratios greater than 1. The previously developed fibre-based finite-element model is validated through a correlation study with experimentally tested RC walls.

Simulation of Pilakoutas and Elnashai (1995) shear wall SW 7

Pilakoutas and Elnashai (1995) tested the RC cantilever wall (SW7) under lateral load. The wall has an aspect ratio of 2·0. The wall has a clear height of 1200 mm, and a cross section of 600 mm × 60 mm. The wall is reinforced with 0·47% flexural web reinforcement and 0·39% shear reinforcement.

The concrete cube strength f_{cu} of the specimen equals 32 MPa. The yield stresses of the longitudinal and transverse reinforcement are 543 MPa and 553 MPa, respectively. Young's modulus of steel is assumed to equal 200 000 MPa.

Figure 4 shows the experimental and analytically derived lateral load–displacement response of wall SW7. The figure reveals that

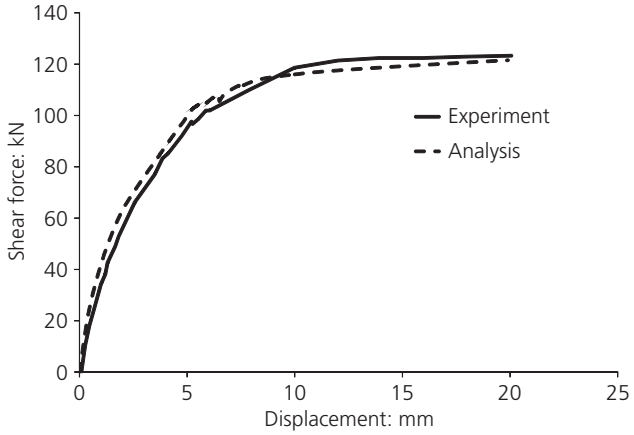

Figure 4. Experimental monotonic load–displacement of wall SW7

the model predicted well the stiffness, as well as the yield and peak load. The response of this specimen was dominated by yielding of the transverse reinforcement prior to shear failure.

Simulation of Peng and Wong (2011) shear walls SW10-100 and SW10-400

Three similar RC walls with the same cross section and reinforcement arrangements and material have been tested under monotonic loading by Peng and Wong (2011). One wall (SW10-0) is tested under only flexure and shear about the major axis of the wall generated by a lateral force acting at the top of the wall with no eccentricity. The other two walls (SW10-100 and SW10-400) are tested under flexure, shear and torsion with an eccentricity of 100 mm and 400 mm, respectively, with respect to the major axis of the wall. All of the wall units have a length of 1000 mm and a width of 150 mm (Figure 5(a)). All of the wall specimens have a height of 1500 mm and are mounted with a loading slab of

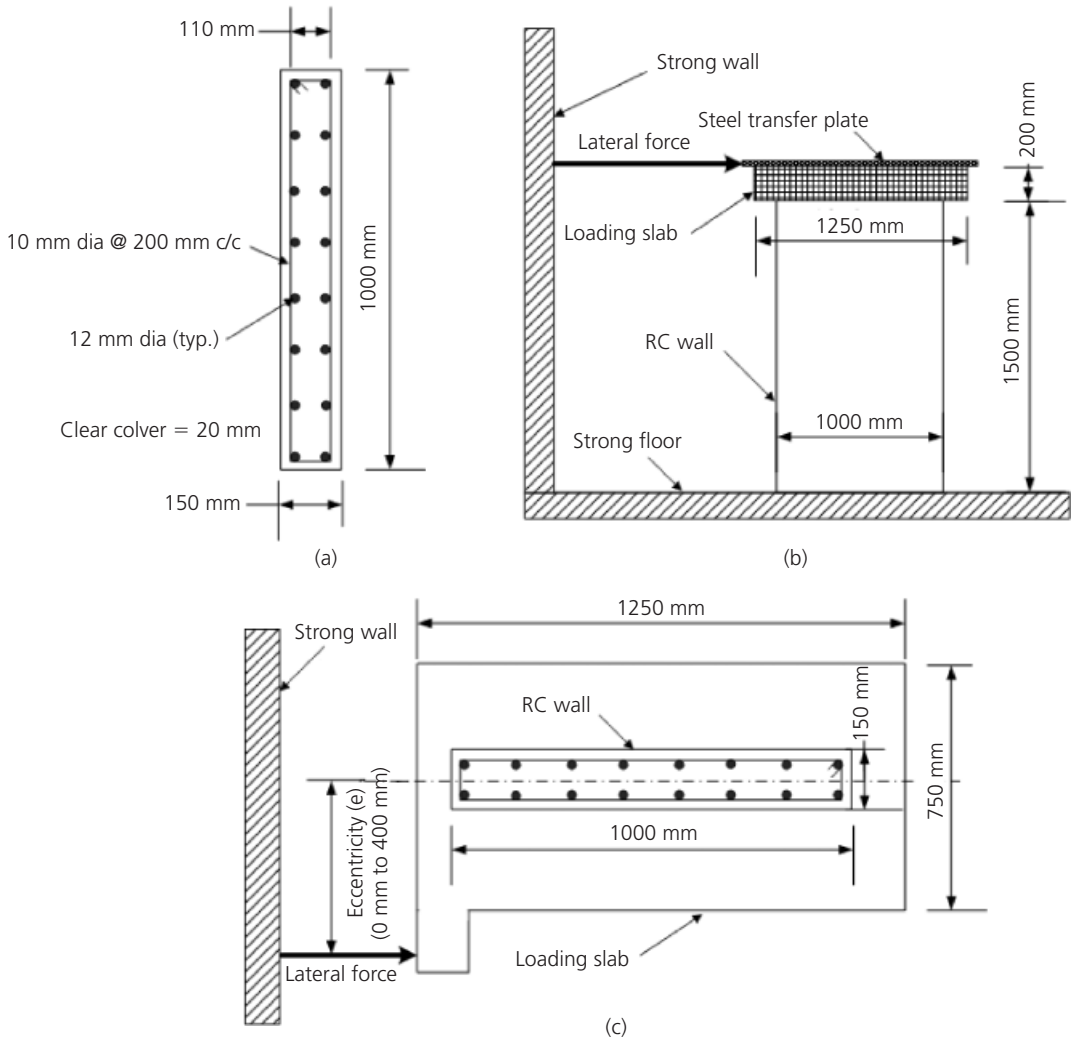

Figure 5. Wall details: (a) cross section, (b) elevation, (c) top view and loading set-up (Peng and Wong, 2011)

1250 mm × 750 mm × 200 mm at the top of the wall. A steel loading transfer plate of 40 mm thick is mounted on top of the loading slab (Figure 5(b)).

The wall is modelled with five Gauss–Lobatto integration points along the element length. Every section represents one integration point, and each section is divided into eight longitudinal and transverse fibres. The top steel transfer plate, the loading slab and the top part of the 300 mm wall portion are modelled with an elastic material. The walls are modelled as a cantilever with fixed base, and the lateral load is applied at the top of the wall, as shown in Figure 5(c). The wall is reinforced with eight longitudinal reinforcements of 12 mm diameter on each face, and with 10 mm diameter transverse reinforcements at 200 mm centre-to-centre spacing. An average compressive strength of concrete of 40·2 MPa, yield strength of longitudinal steel of 535 MPa and yield strength of transverse reinforcement of 564 MPa are used in the analysis. A clear cover of 20 mm is used in the analysis.

Figure 6 shows the wall SW10-0 flexure–shear response without torsional effect. Wall SW10-0 failed under ductile flexure with the formation of a plastic hinge at the bottom of the wall. At the peak load, both the longitudinal and transverse steel yielded at the bottom of the wall. The fibre beam element was able to predict the cracking, yielding, ultimate load and corresponding displacement ductility accurately compared to the experimental results.

Figure 7 shows the shear force–displacement response of wall SW10-100. This wall failed under ductile flexure failure because the bending behaviour dominated the torsional behaviour of the wall. A plastic hinge was formed at the bottom of the wall. At the peak load, both the longitudinal and transverse steel yielded at the bottom of the wall. The strength, stiffness and ductility are reduced in the presence of the torque. The fibre beam element was able to predict the cracking and yielding loads and corresponding displacements rather well, but a deviation was found at the peak load because this wall failed prematurely during the experiment due to lack of the required strength of the bottom slab. Owing to the applied torque, the flexural strength of the wall is reduced by about 28%, and the flexural ductility is reduced by 48% compared to the SW10-0 wall response.

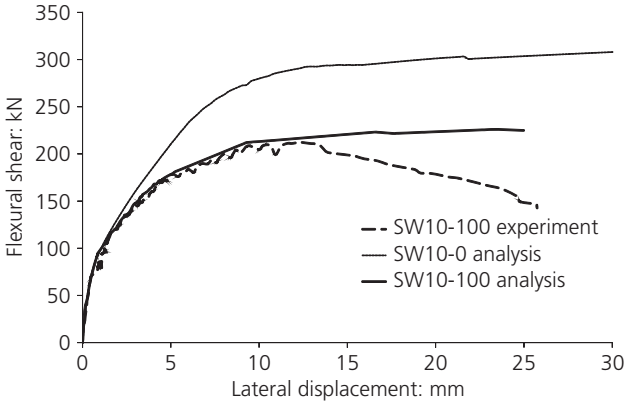

Figure 7. Load–displacement response of wall SW10-100

Figure 8 shows the shear force–displacement response of wall SW10-400. This wall failed under the domination of shear over flexure, with the formation of a plastic hinge at 400 mm from the bottom of the wall. At the peak load, the longitudinal and transverse steel yielded at the bottom and middle of the wall. The strength, stiffness and ductility are reduced in the presence of the torque. The fibre beam element was able to predict the load–deformation response well. From the figure, it is apparent that with the increase of the torque, the flexural strength is reduced by 60% and the flexural ductility is reduced by 90% compared to the SW10-0 wall response.

Figure 9 shows the response of the torque–angle of twist response for wall SW10-100. The fibre beam element was able to capture the cracking, yielding and peak behaviour rather accurately, but the post-peak response did not match well because of the premature experimental failure of the wall.

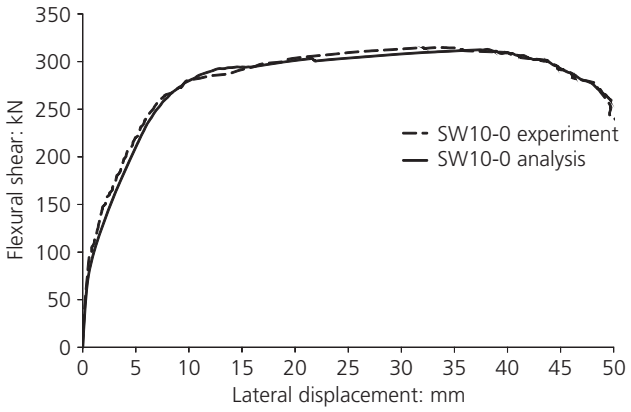

Figure 6. Load–displacement response of wall SW10-0

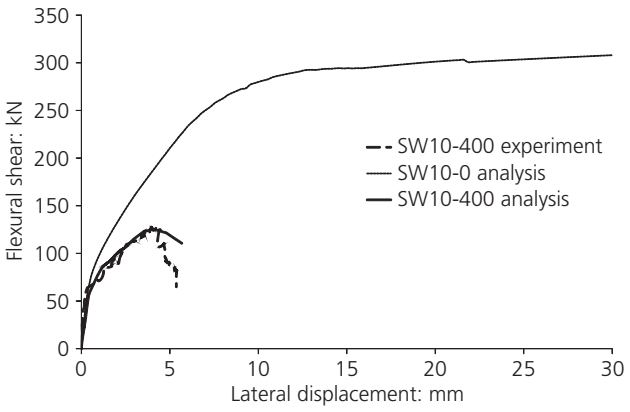

Figure 8. Load–displacement response of wall SW10-400

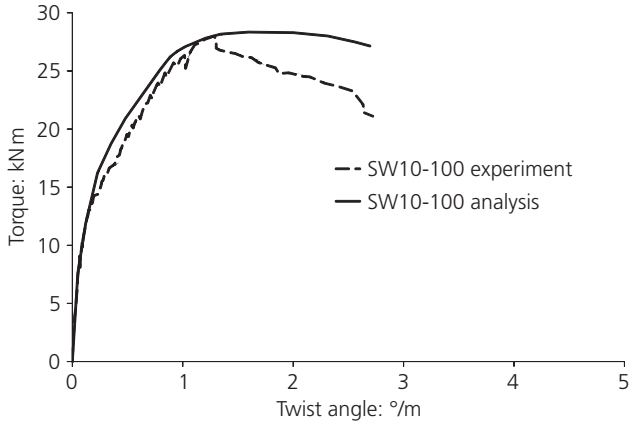

Figure 9. Torque–twist response of wall SW10-100

Figure 10 shows the torque–angle of twist response of wall SW10-400. This wall is loaded with about 120% torsional load higher than the SW10-100 wall. The torsional strength, stiffness and ductility are reduced with the increase of the torque. The fibre beam element was able to capture the cracking, yielding, peak load and corresponding twisting angles rather well. At first yield, the transverse reinforcement yielded, but at the peak load, both the longitudinal and transverse reinforcements yielded.

Conclusions

The analysis conducted in this study on shear walls subjected to combined loadings has served to address the effect of torsion on wall behaviour. A 3D fibre beam element is developed with Timoshenko beam formulation to incorporate shear effects. The combination of an appropriate finite-element formulation and the SMM provided a simple and reliable analytical tool for evaluating the behaviour of walls subjected to combined loadings, including torsion. The displacement control scheme is stable, and is able to predict the pre-peak and post-peak behaviour of the hysteresis loop. With the increase of the torque to moment ratio, the torsional stiffness degrades rapidly as compared to the flexural stiffness, and the flexural energy dissipation is reduced considerably. The new model accurately predicted the stiffness, cracking, yield point, ultimate strength, energy dissipation and failure modes of the wall specimens, confirming its applicability as an analysis and design tool for engineers.

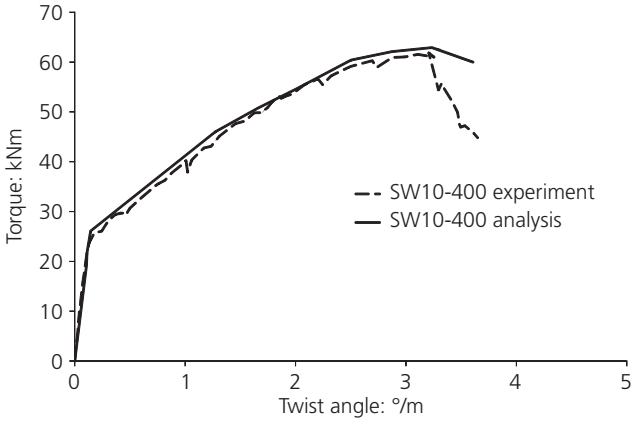

Figure 10. Torque–twist response of wall SW10-400

Acknowledgements

Financial support for this project provided by the National Science Foundation under grant number CMMI-0530737 is gratefully acknowledged. However, opinions expressed in this paper are those of the writers and do not necessarily reflect those of the sponsors. The authors would like to thank Dr Wong Yuk-Lung and Peng Xiao-Ning at Hong Kong Polytechnic University for providing the experimental data of the wall specimens.

REFERENCES

Bairan JM and Mari AR (2006) Coupled model for the non-linear analysis of anisotropic sections subjected to general 3D loading. *Computers and Structures* **84(31–32)**: 2254–2263.

Bairan JM and Mari AR (2007) Multiaxial-coupled analysis of RC cross-sections subjected to combined forces. *Engineering Structures* **29(8)**: 1722–1738.

Belarbi A and Hsu TTC (1994) Constitutive laws of concrete in tension and reinforcing bars stiffened by concrete. *ACI Structural Journal* **91(4)**: 465–474.

Belarbi A and Hsu TTC (1995) Constitutive laws of softened concrete in biaxial tension-compression. *ACI Structural Journal* **92(5)**: 562–573.

Bolander J and Wight J (1991) Finite element modeling of shear-wall-dominant buildings. *Journal of Structural Engineering* **117(6)**: 1719–1739.

Cocchi GM and Volpi M (1996) Inelastic analysis of reinforced concrete beams subjected to combined torsion, flexural and axial loads. *Computers and Structures* **61(3)**: 479–494.

Gregori JN, Sosa PM, Prada MAF and Filippou FC (2007) A 3D numerical model for reinforced and prestressed concrete elements subjected to combined axial, bending, shear and torsion loading. *Engineering Structures* **29(12)**: 3404–3419.

Hsu TTC and Zhu RRH (2002) Softened membrane model for reinforced concrete elements in shear. *ACI Structural Journal* **99(4)**: 460–469.

Hsu TTC, Belarbi A and Pang X (1995) A universal panel tester. *Journal of Testing and Evaluation* **23(1)**: 41–49.

Jeng CH and Hsu TTC (2009) A softened membrane model for torsion in reinforced concrete members. *Engineering Structures* **31(9)**: 1944–54.

Kupfer HB, Hildorf HK and Rusch H (1969) Behavior of concrete under biaxial stresses. *ACI Structural Journal* **66(8)**: 656–666.

Lefas ID and Kotsovos MD (1990) NLFE Analysis of R.C. structural walls and design implications. *Journal of Structural Engineering* **116(1)**: 146–164.

Mazars J, Kotronis P and Davenne L (2002) A new modeling strategy for the behavior of shear walls under dynamic

loading. *Earthquake Engineering and Structural Dynamics* **31(4)**: 937–954.

Mullapudi TRS (2010) *Seismic Analysis of Reinforced Concrete Structures Subjected to Combined Axial, Bending, Shear and Torsional Loads*. PhD thesis, Department of Civil and Environmental Engineering, University of Houston, Houston, USA.

Mullapudi TRS and Ayoub AS (2009) *Fiber Beam Element Formulation Using the Softened Membrane Model*. SP-265, ACI, Farmington Hills, MI, USA, pp. 283–308.

Mullapudi TRS and Ayoub AS (2010) Modeling of the seismic behavior of shear-critical reinforced concrete columns. *Journal of Engineering Structures* **32(11)**: 3601–15.

Orakcal K and Wallace JW (2006) Flexural modeling of reinforced concrete walls – model calibration. *ACI Structural Journal*, **103(2)**: 196–206.

Peng XN and Wong YL (2011) Experimental study on reinforced concrete walls under combined flexure, shear and torsion. *Magazine of Concrete Research* **63(6)**: 459–471.

Pilakoutas K and Elnashai A (1995) Cyclic behavior of reinforced concrete cantilever walls. Part I: Experimental results. *ACI Structural Journal* **92(3)**: 271–281.

Spacone E, Filippou FC and Taucer FF (1996) Fiber beam-column model for nonlinear analysis of R/C frames. Part I formulation. *Earthquake Engineering and Structural Dynamics* **25(7)**: 711–725.

Taylor RL (2005) *FEAP User Manual v2.0*. Department of Civil and Environmental Engineering, University of California, Berkeley. See http//www.ce.berkeley.edu/~rlt/feap/ (accessed 16/06/2012).

Vecchio FJ (1992) Finite element modeling of concrete expansion and confinement. *Journal of Structural Engineering* **118(9)**: 2390–2405.

Vecchio FJ and Selby RG (1991) Toward compression-field analysis of reinforced concrete solids. *Journal of Structural Engineering* **117(6)**: 1740–1758.

Zhu RH and Hsu TTC (2002) Poisson effect of reinforced concrete membrane elements. *ACI Structural Journal* **99(5)**: 631–640.

WHAT DO YOU THINK?

To discuss this paper, please submit up to 500 words to the editor at www.editorialmanager.com/macr by 1 August 2013. Your contribution will be forwarded to the author(s) for a reply and, if considered appropriate by the editorial panel, will be published as a discussion in a future issue of the journal.